ELEMENTA
Science of the Anthropocene

Prend, CJ, et al. 2025. Observing system requirements for measuring high-frequency air–sea fluxes in the Southern Ocean. *Elem Sci Anth*, 13: 1. DOI: https://doi.org/10.1525/elementa.2024.00061

RESEARCH ARTICLE

Observing system requirements for measuring high-frequency air—sea fluxes in the Southern Ocean

Channing J. Prend[1,2,*], Marcel D. du Plessis[3], Matthew R. Mazloff[4], Lovisa Sunnercrantz[3], Sebastiaan Swart[3,5], and Sarah T. Gille[4]

Southern Ocean air–sea fluxes are a critical component of the climate system but are historically undersampled due to the remoteness of the region. While much focus has been placed on interannual flux variability, it has become increasingly clear that high-frequency fluctuations, driven by processes like storms and (sub-)mesoscale eddies, play a nonnegligible role in longer-term changes. Therefore, collecting high-resolution in situ flux observations is crucial to better understand the dynamics operating at these scales, as well as their larger-scale impacts. Technological advancements, including the development of new uncrewed surface vehicles, provide the opportunity to increase sampling at small scales. However, determining where and when to deploy such vehicles is not trivial. This study, conceived by the Air–Sea Fluxes working group of the Southern Ocean Observing System, aims to characterize the statistics of high-frequency air–sea flux variability. Using statistical analyses of atmospheric reanalysis data, numerical model output, and mooring observations, we show that there are regional and seasonal variations in the magnitude and sign of storm- and eddy-driven air–sea flux anomalies, which can help guide the planning of field campaigns and deployment of uncrewed surface vehicles in the Southern Ocean.

Keywords: Southern Ocean, Air–sea fluxes, Synoptic variability, Eddy dynamics

1. Introduction

The Southern Ocean plays an outsized role in oceanic uptake of heat and carbon (Frölicher et al., 2015; Roemmich et al., 2015; Williams et al., 2023). Therefore, air–sea fluxes in this region have a particularly large influence on global climate (Swart et al., 2023). Despite their importance within the climate system, Southern Ocean air–sea fluxes are historically undersampled due to the challenges associated with collecting data in this remote and harsh environment (Gille et al., 2016; Swart et al., 2019). Sustained in situ flux measurements have been collected by just two moorings in the sub-Antarctic, one of which is no longer active (Schulz et al., 2012; Tamsitt et al., 2020), while high-frequency in situ flux measurements have been confined to regional research expeditions (Butterworth and Miller, 2016; Bharti et al., 2019; Pezzi et al., 2021; Rodrigues et al., 2023). Furthermore, reanalysis products are known to have large uncertainties in the Antarctic, particularly for transient extreme events (Bourassa et al., 2013; Potter et al., 2018). Expanded data coverage, in both space and time, is needed to evaluate these biases and better understand the mechanisms of oceanic heat uptake (Cronin et al., 2019; Swart et al., 2019).

In recognition of this key observational gap, the Southern Ocean Observing System (SOOS) established an Air–Sea Fluxes working group (SOFLUX) in 2015 (Gille et al., 2016). Since its inception, SOFLUX has synthesized community priorities (Swart et al., 2019) and—in collaboration with the SOOS Observing System Design (OSD) working group—facilitated observing system simulation experiments (OSSEs) related to Southern Ocean air–sea exchange (Wei et al., 2020). OSSEs are an essential tool to evaluate and formulate new field campaigns, and previous Southern Ocean studies have investigated optimal mooring placement (Wei et al., 2020) or optimal array design for autonomous profiling float deployments (Kamenkovich et al., 2017; Mazloff et al., 2018; Chamberlain et al., 2023). Naturally, establishing what constitutes "optimal" in the context of these studies is necessary. In all of the previously cited Southern Ocean OSSEs, the

[1] School of Oceanography, University of Washington, Seattle, WA, USA
[2] Environmental Science & Engineering, California Institute of Technology, Pasadena, CA, USA
[3] Department of Marine Sciences, University of Gothenburg, Gothenburg, Sweden
[4] Scripps Institution of Oceanography, University of California San Diego, La Jolla, CA, USA
[5] Department of Oceanography, University of Cape Town, Rondebosch, South Africa

* Corresponding author:
Email: cprend@uw.edu

acknowledged priority was to constrain the large-scale, interannual variability either in the air–sea fluxes directly or in related properties such as upper-ocean heat and carbon content. This priority is understandably motivated by the need to capture climate signals and long-term trends associated with anthropogenic forcing.

However, air–sea fluxes vary across a wide range of scales (Cronin et al., 2019; Swart et al., 2019). For example, extreme heat loss events (more than -300 W m^{-2} daily averages) can be tied to synoptic storms (Ogle et al., 2018; Tamsitt et al., 2020). Ocean property gradients associated with eddies and fronts can lead to sharp transitions in air–sea exchange (Seo et al., 2023). Moreover, there is growing evidence that this high-frequency flux variability has a rectified effect on the longer time scales (Resplandy et al., 2014; Monteiro et al., 2015; Cronin et al., 2019; Nicholson et al., 2022). For example, Ogle et al. (2018) showed that the interannual variability in mixed-layer depth (MLD) at one of the Southern Ocean flux mooring locations could be linked to surface cooling from just a small number of storm events. This linkage implies that resolving high-frequency processes may be necessary to understand and interpret longer-term changes in the climate system.

With this context in mind, there is a pressing need for more air–sea flux observations from transient conditions associated with storms and eddies. Meeting this need poses challenges due to the high sea states and the episodic nature of these events. However, obtaining these measurements is critical to reduce uncertainties in reanalysis products and quantify the rectification of high-frequency variability into longer time scales. Furthermore, the rise in process studies using autonomous technologies requires a better understanding of regional and temporal variations in high-frequency processes, which will enable future studies to select optimal deployment locations and times. Therefore, this study, which is a product of SOFLUX, aims to characterize air–sea flux anomalies associated with synoptic storms and oceanic mesoscale variability in order to establish the observing system requirements for sampling these high-frequency fluctuations. We show that there are distinct regional differences in the dominant scale and leading drivers of high-frequency air–sea flux variability. These differences serve as important context for designing future field campaigns to the Southern Ocean.

2. Data and methods

2.1. Observational datasets

In this study, we used daily averages from the 1/4° resolution European Centre for Medium-Range Weather Forecasts (ECMWF) Reanalysis v5 (ERA5) product (Hersbach et al., 2020). The net air–sea heat flux (Q_{net}) was taken to be the sum of the shortwave, longwave, latent, and sensible heat fluxes. Together, the shortwave and longwave components make up the radiative flux, while the latent and sensible components comprise the turbulent flux. We concentrated the analysis on daily Q_{net} during the period from 2013 to 2018 (**Figure 1a**) in order to compare with the Biogeochemical Southern Ocean State Estimate (B-SOSE) described in Section 2.2 (Figure S1).

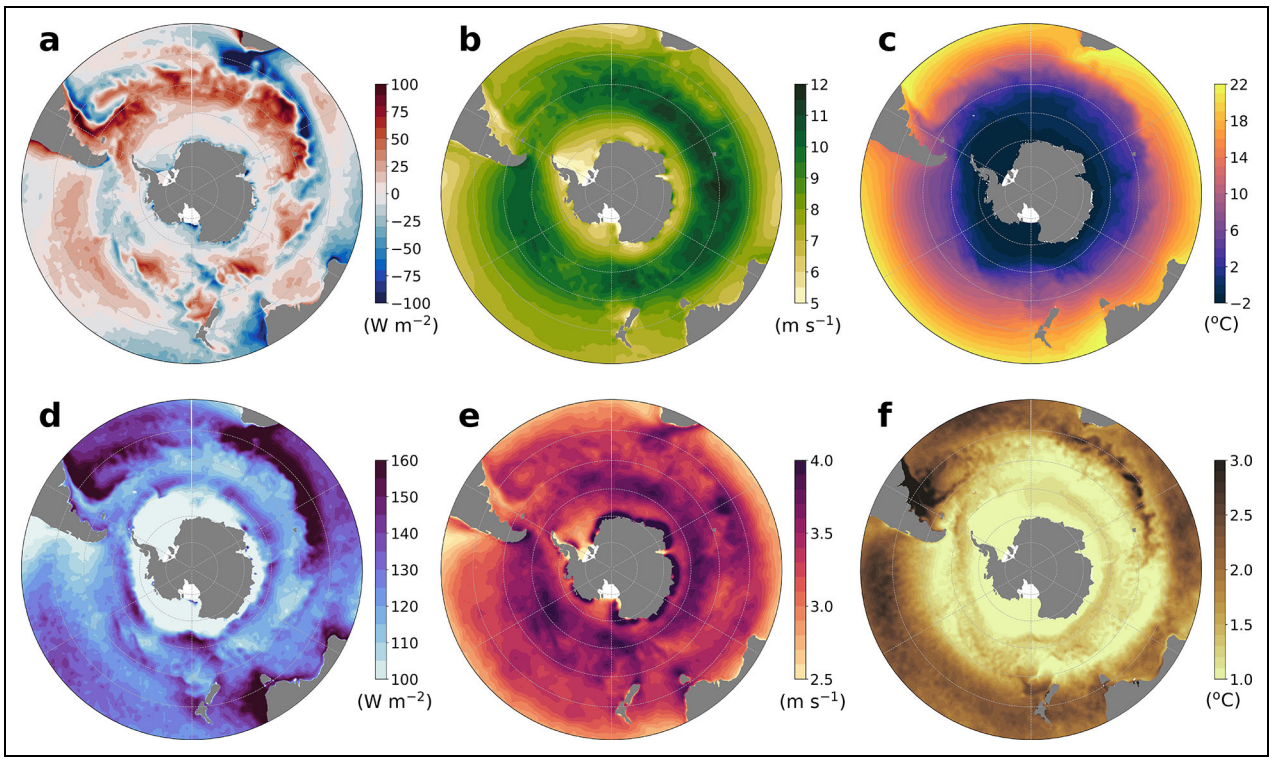

Figure 1. Patterns of air–sea heat flux, wind speed, and sea surface temperature. Mean values, for the period 2013–2018, of (a) net air–sea heat flux from ERA5 reanalysis, (b) wind speed from the Cross-Calibrated Multi Platform (CCMP) vector wind product, and (c) sea surface temperature (SST) from the NOAA Optimum Interpolated SST product, with (d–f) the standard deviation of the respective parameters.

Although this 6-year period is much shorter than the full ERA5 time span, our focus is on high-frequency processes. Moreover, the main conclusions of this work are consistent with results based on ERA5 data from a longer 24-year period (see Text S1).

We also used daily averages from the Cross-Calibrated Multi Platform (CCMP) ocean surface winds. CCMP winds are provided on a 25 × 25 km grid at 6-hourly resolution. Because CCMP combines ocean surface wind retrievals from multiple platforms, it matches in situ observations better than any individual scatterometer, particularly at high frequencies (Atlas et al., 2011). For sea surface temperature (SST), we used daily fields from Version 2.1 of the NOAA Optimum Interpolated SST product (Huang et al., 2021). We have also plotted 2013–2018 mean eddy kinetic energy derived from sea level anomaly fields in the altimetry product distributed by the Copernicus Marine Service (http://doi.org/10.48670/moi-00148). All gridded products were interpolated onto the same 1/4° grid as the ERA5 data.

To supplement the reanalysis products, we analyzed in situ data from the Southern Ocean Flux Station (SOFS), an air–sea flux mooring located in the sub-Antarctic at 47°S, 142°E (yellow star in **Figure 2**), which is part of the Southern Ocean Time Series Observatory. The mooring is equipped with dual climate-quality Air–Sea Interaction Meteorology (ASIMET) systems, which included direct measurements of radiative fluxes, and the surface variables needed to calculate turbulent fluxes using bulk formulae (Schulz et al., 2012). The mooring was first deployed in 2010, and provides the longest record of in situ flux measurements from the Southern Ocean, although there are significant gaps due to sensor and mooring failures. Here, we used daily averages computed from the hourly observations.

2.2. Model output

We also utilized air–sea heat fluxes, and other fields, from B-SOSE. B-SOSE is a data-assimilating model (Verdy and Mazloff, 2017) that constrains the Massachusetts Institute of Technology general circulation model (MITgcm) solution (Marshall et al., 1997) with satellite and hydrographic measurements. The configuration used in this analysis, Iteration 133, has 1/6° horizontal resolution, 52 unevenly spaced vertical levels, and runs from January 1, 2013 to December 31, 2018. This iteration of B-SOSE is publicly available (http://sose.ucsd.edu). Validation of air–sea fluxes from an earlier version of SOSE is provided in Cerovečki et al. (2011), which includes comparison to several different reanalysis products. A previous iteration of B-SOSE was also used to estimate the decorrelation lengths of low-frequency air–sea flux variability (Mazloff et al., 2018). The model is a useful complement to the reanalysis data because it is dynamically consistent and has finer horizontal resolution. B-SOSE fields compare well with the reanalysis, which is unsurprising as the atmospheric state in the model is prescribed from adjusted ERA5 reanalysis.

2.3. Correlation scales

In order to characterize the space and time scales of high-frequency Q_{net}, wind, and SST variability, we first removed the annual cycle by least-squares fitting a sinusoidal function with a period of 365.25 days to the time series at each

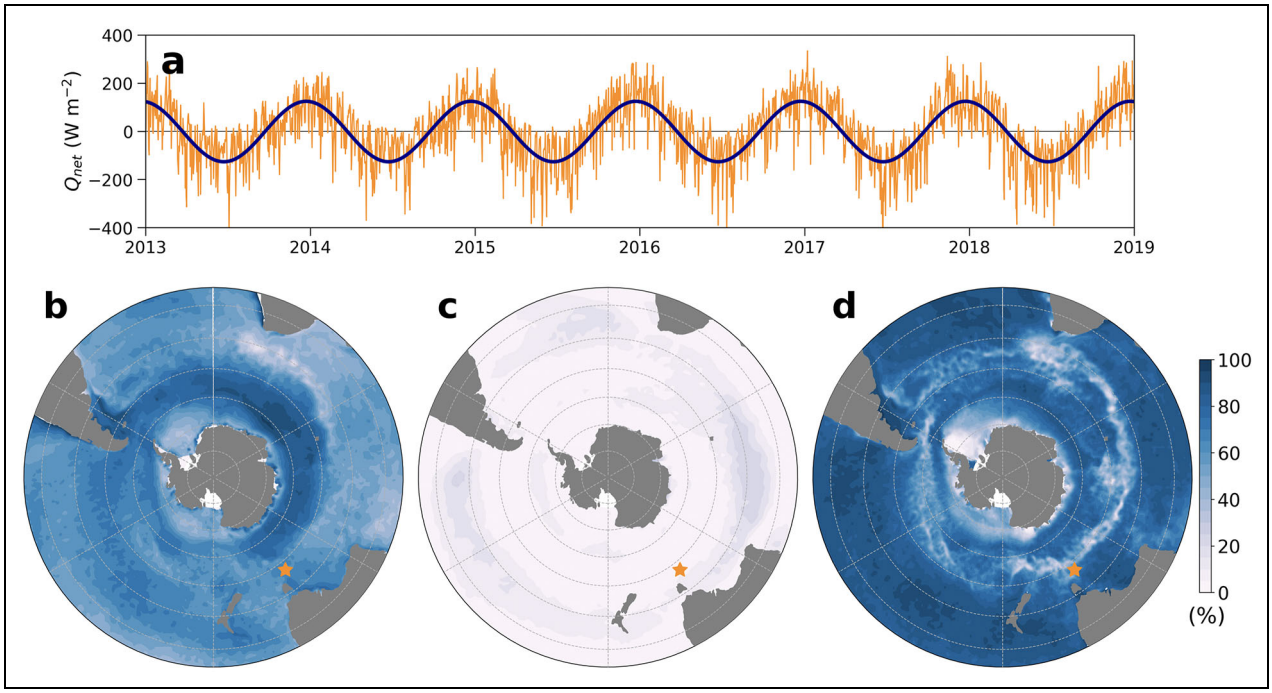

Figure 2. Explanatory power of the seasonal cycle. (a) Example time series of daily air–sea heat flux (Q_{net}) from ERA5 (orange) at the Southern Ocean Flux Station mooring location (marked by an orange star in the lower panels) and the least-squares fitted annual cycle (navy). Percentage of total variance explained by the annual cycle for (b) Q_{net}, (c) 10 m wind speed, and (d) sea surface temperature.

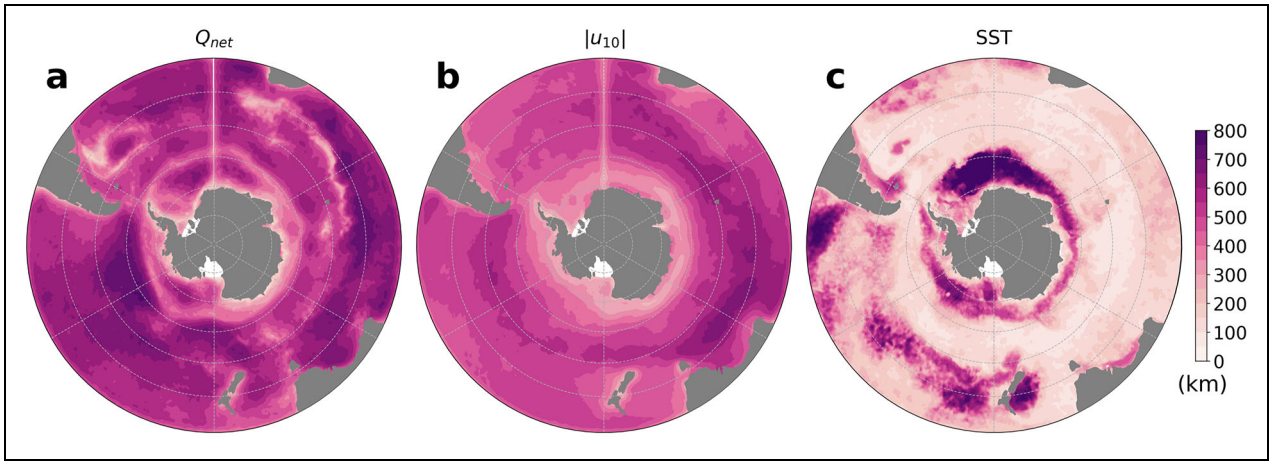

Figure 3. Decorrelation length scales. Decorrelation lengths (km) for the high-frequency component of (a) net air–sea heat flux (Q_{net}), (b) 10 m wind speed ($|u_{10}|$), and (c) sea surface temperature (SST).

grid cell (e.g., **Figure 2a**) and then subtracting it from the full signal. This sinusoidal representation of the seasonal cycle explains up to 90% of the total SST variance across much of the Southern Ocean (**Figure 2d**), except notably in the core of the Antarctic Circumpolar Current (ACC) and in boundary current regions like the Brazil–Malvinas Confluence and the Agulhas Retroflection. These exceptions are consistent with the fact that a more energetic eddy field produces greater high-frequency variability (see Sections 3.1 and 3.3). For Q_{net} and wind speed, the variance explained by the seasonal cycle is lower compared to SST, about 40%–50% and 10%–20%, respectively (**Figure 2b** and **2c**). We then applied a 90-day high-pass filter to the deseasonalized time series to isolate the high-frequency component. From these filtered data, we computed decorrelation length and time scales of the high-frequency Q_{net}, wind speed, and SST. The decorrelation time scale was defined, at each grid point, as the e-folding scale of the autocorrelation function. The decorrelation length scale was determined from the spatial autocorrelation as the square root of the area over which the correlation coefficient (r) exceeded a threshold value of 0.8 (Prend et al., 2022). This definition does not allow for anisotropy; however, the spatial autocorrelation of the high-pass filtered fields appears to be approximately isotropic (Text S2, Figure S2). Similar length scales were obtained for a range of threshold r values from 0.7 to 0.9 (not shown). While there are alternative methods of defining decorrelation lengths (e.g., Mazloff et al., 2018; Chu et al., 2024), here we have opted for simplicity such that the results can be interpreted easily and serve as the foundation for further investigation.

3. Results and discussion

3.1. Scales of variability

There are clear spatial patterns in the mean and standard deviation of Q_{net}, wind speed, and SST (**Figure 1**). For example, the standard deviation of Q_{net} (**Figure 1d**) is elevated in energetic regions with high climatological eddy kinetic energy (EKE; Section 3.3) and SST variance (**Figure 1f**), such as the Brazil–Malvinas Confluence and the Agulhas Retroflection and Return Current. The decorrelation lengths of high-frequency Q_{net} are much smaller (about 100 km) in these locations (**Figure 3a**), indicating a key role for mesoscale eddies in driving the air–sea flux variability. This role is presumably due to eddy-driven SST anomalies modulating air–sea property gradients (Villas Bôas et al., 2015) although regionality in air temperature variance may also play a role. Throughout the rest of the Southern Ocean, the Q_{net} decorrelation lengths are generally >500 km, consistent with synoptic storm variability. Despite this distinct regionality in decorrelation lengths, the Q_{net} decorrelation time scales are approximately 2 days everywhere (**Figure 4a**), except in the seasonal ice zone where ERA5 biases may be higher (King et al., 2022).

The patterns for wind speed and SST variability are not the same as for Q_{net}. Mean wind speed displays a strong meridional gradient (as expected based on the position of the westerlies), but the standard deviation is very patchy (**Figure 1e**), apart from a fairly consistent band of high variability around 50–60°S. As noted above, wind speed has a small percentage of variance explained by the seasonal cycle (about 10%), and the decorrelation length and time scales of the high-frequency component are largely spatially uniform across the Southern Ocean (about 500 km, 1–2 days). SST, on the other hand, is primarily seasonal (>80% of the total variance in most locations). High SST standard deviation generally aligns with high Q_{net} standard deviation; however, unlike Q_{net}, the decorrelation lengths for high-frequency SST are small (around 100–200 km) nearly everywhere, not just in boundary currents. Notably, the decorrelation time scales for SST are also longer (>30 days), highlighting the disparity between the time scale of the forcing and of the ocean response (Carranza et al., 2018; Whitt et al., 2019).

3.2. Storm impacts

Away from energetic boundary currents and ACC fronts, the decorrelation scales of high-frequency Q_{net} are consistent with synoptic storm variability. Storms can impact radiative fluxes via cloud processes, as well as turbulent

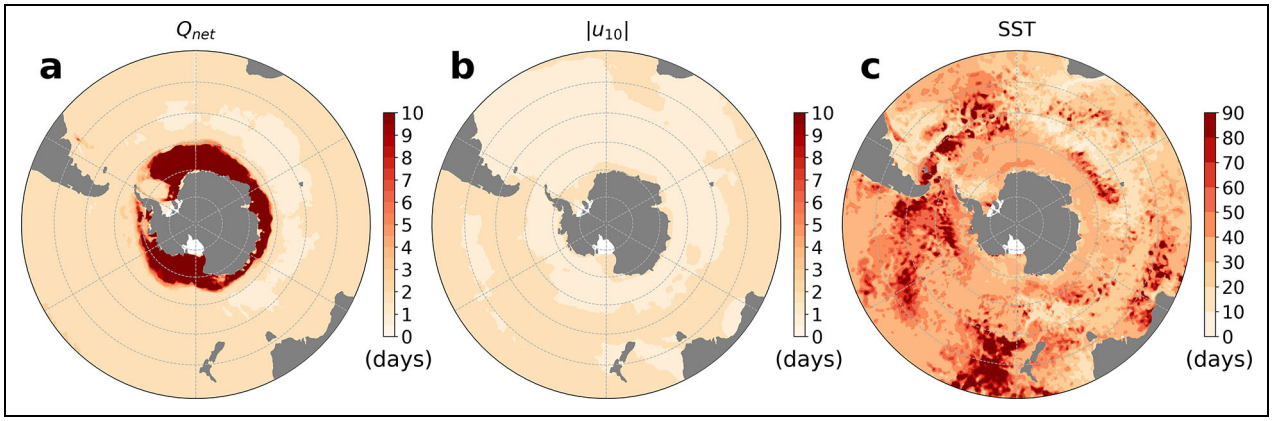

Figure 4. Decorrelation time scales. Decorrelation times (days) for the high-frequency component of (a) net air–sea heat flux (Q_{net}), (b) 10 m wind speed ($|u_{10}|$), and (c) sea surface temperature (SST). Note that the axis extent differs in panel c because the decorrelation times for SST are 1–2 orders of magnitude larger than for Q_{net} and $|u_{10}|$.

fluxes by increasing transfer coefficients (due to high wind speeds), or by altering air–sea temperature and humidity gradients (Bharti et al., 2019; Cronin et al., 2019). Observations from the SOFS mooring showed that episodic turbulent heat loss events can be associated with storm-driven advection of cold, dry air from the south (Schulz et al., 2012) or of dry air from the north (Tamsitt et al., 2020). In these cases, intensified latent heat loss resulted from an increase in the air–sea humidity difference and strong winds. However, whether the conditions at the SOFS mooring location can be generalized to the entire Southern Ocean, or how extreme events vary at seasonal and interannual time scales, is unclear.

To investigate these questions, we adopted a simple storm classification method based on daily mean wind speed (Hodges et al., 2011). Namely, a threshold of 10 m s^{-1} was used to define storm events. Based on this classification, the SOFS mooring data show a 42 W m^{-2} increase in latent heat-flux magnitude and an 8 W m^{-2} increase in sensible heat-flux magnitude during storm events (**Figure 5**). These increases are due primarily to the stronger wind speeds, rather than changes in the air–sea temperature and humidity gradients (**Figure 5**). However, these results may only reflect a narrow band in the subpolar Southern Ocean, given the strong meridional gradient in storm occurrences (**Figure 6a**) and storm-related air–sea flux (**Figure 6b**). For example, at low latitudes (around 30–45°S), storms coincide with intense cooling. Whereas in the core of the ACC, storms are associated with ocean warming on average, particularly in the Atlantic and Indian sectors. This association could be due to mid-latitude cyclones advecting warm air southward or storm-driven entrainment bringing warm Circumpolar Deep Water into the surface mixed-layer (Nicholson et al., 2022).

In addition to regionality, there is also seasonality in storm events (Nakamura and Shimpo, 2004). For instance, at the SOFS mooring, the months with the maximum and minimum number of storm days are September (53%) and February (24%), respectively. Across the Southern Ocean, storms exhibit seasonal fluctuations, despite the small percentage of annual wind speed variance explained by the seasonal cycle (**Figure 2c**). Specifically, storms are more frequent in winter compared to summer (**Figure 7a** and **7b**), with both seasons displaying the same meridional gradient, which is related to the position of the westerlies. Beyond differences in storm prevalence, there are also seasonal changes in the associated Q_{net} anomalies (**Figure 7c** and **7d**). In both seasons, storms coincide with strong cooling at subtropical latitudes. However, in the ACC (around 50–60°S), storm-driven Q_{net} anomalies are much smaller in magnitude and even positive in summer across much of the Atlantic and Indian sectors. In contrast, in winter, positive Q_{net} anomalies are confined to the seasonal sea ice zone.

The latitudinal dependence of the amplitude and sign of Q_{net} anomalies during storm events may be explained, in part, by the poleward transition from temperature- to salinity-driven stratification. In the subtropics, entrainment acts to cool the surface ocean by mixing up cold subsurface waters. However, in high-latitude, salt-stratified environments, warm waters underlie the mixed layer, and thus, entrainment may induce surface warming. Therefore, different regions can exhibit an opposite-signed temperature response to storm-driven mixing (du Plessis et al., 2023). Collocated observations of the air–sea interface and ocean interior (Nicholson et al., 2022), from a range of latitude bands, are necessary to probe these mechanisms further. Moreover, whether the persistence or intensity of storms exerts a greater influence over the seasonal and longer-term heat-flux variability is unclear. For example, although there are fewer storms in the low-latitude Southern Ocean, the corresponding Q_{net} anomalies are large and could potentially contribute to the low-frequency variations.

Determining the net impact of synoptic variability on longer time scales requires sustained measurements. Storm events have been suggested to be central to the interannual variability of turbulent heat fluxes in parts of the Southern Ocean (Ogle et al., 2018; Tamsitt et al., 2020; Yang et al., 2022). This importance could be due to interannual fluctuations in the quantity and severity of

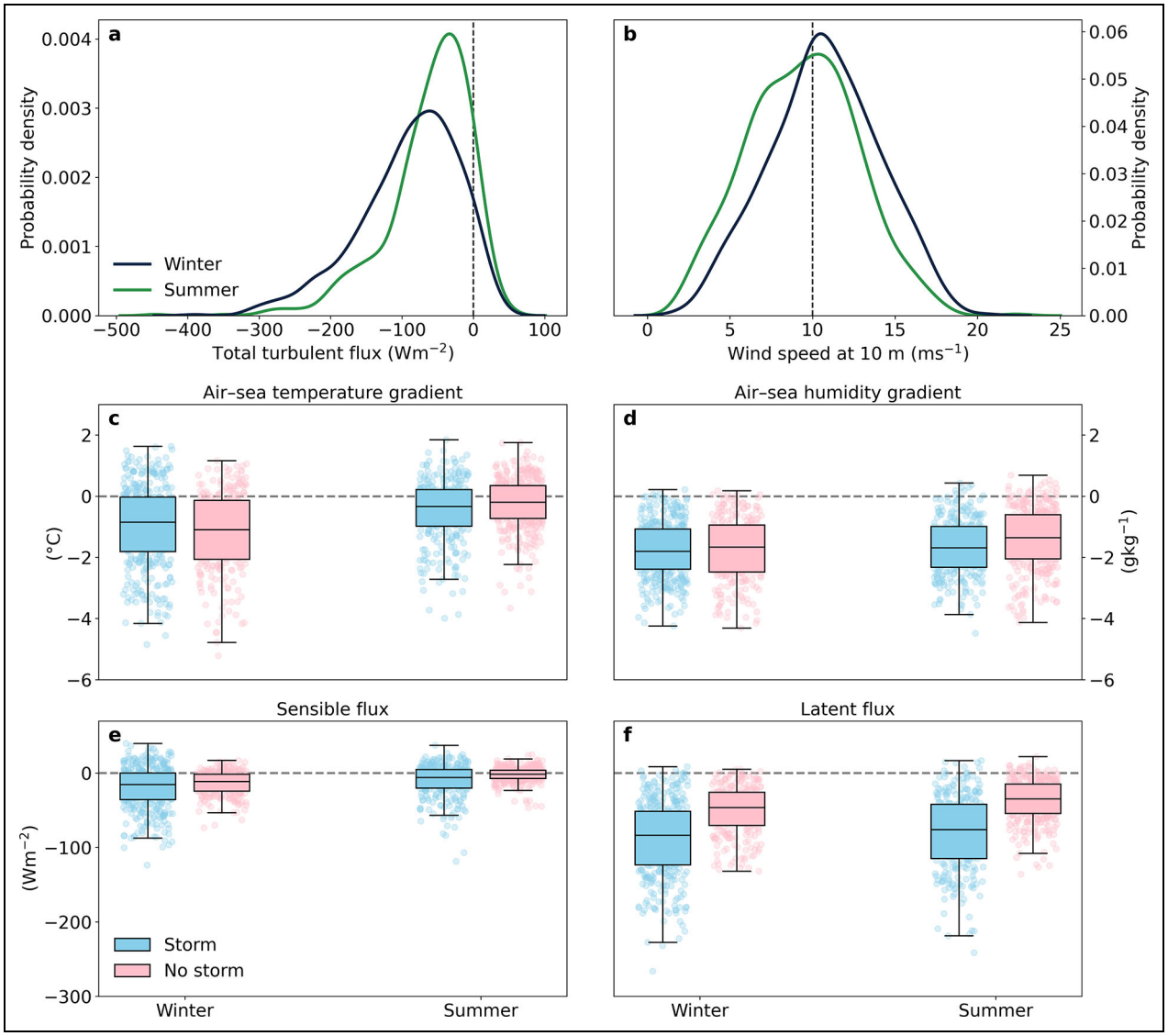

Figure 5. Storm statistics from mooring observations. Probability density functions of (a) turbulent heat flux and (b) 10 m wind speed at the Southern Ocean Flux Station mooring for winter (June–August; navy) and summer (December–February; green). Box plots of air–sea (c) temperature and (d) humidity gradients, as well as (e) sensible and (f) latent heat fluxes. Box plots are separated by season and storm (blue) versus non-storm (pink) days.

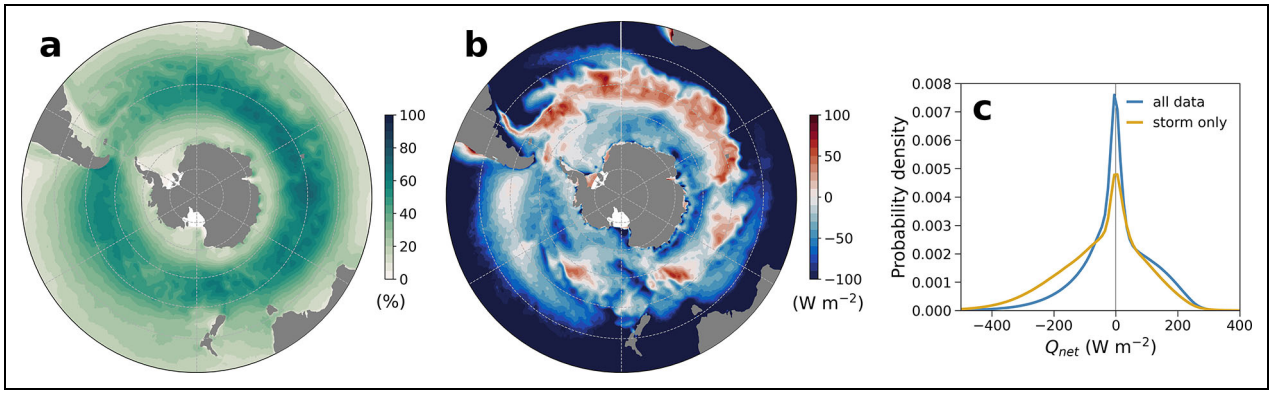

Figure 6. Storm frequency and heat-flux anomalies. (a) Percentage of days with daily mean wind speed greater than 10 m s^{-1} (i.e., storm days), (b) mean air–sea heat flux (Q_{net}) on storm days, and (c) probability density functions of daily Q_{net} for all ERA5 data south of 30°S (blue) and for storm days only (yellow).

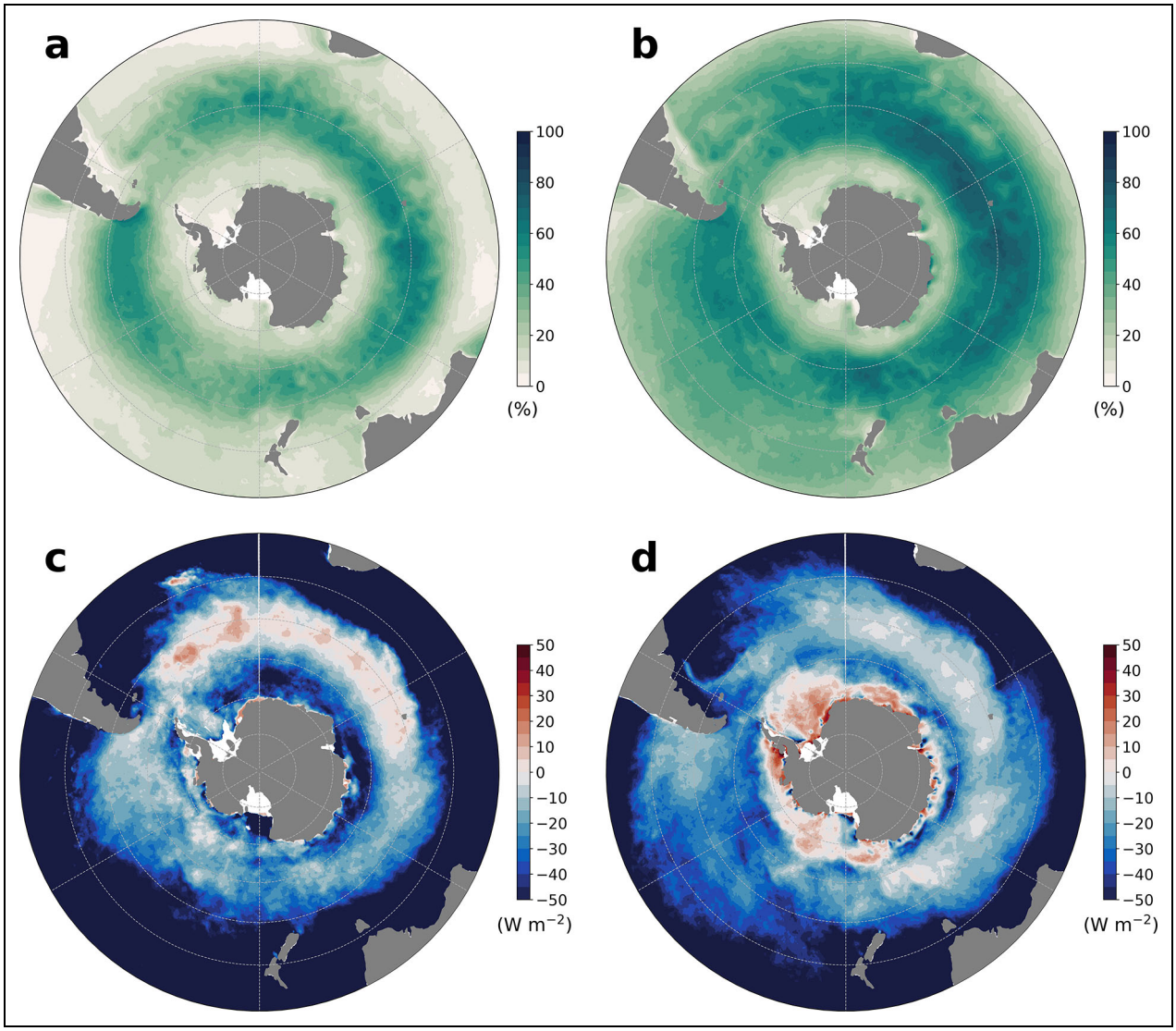

Figure 7. Seasonality of storm frequency and heat-flux anomalies. Percentage of days in (a) summer (December–February) and (b) winter (June–August) with daily mean wind speed greater than 10 m s^{-1} (i.e., storm days). Mean storm-driven air–sea heat-flux (Q_{net}) anomaly (from the seasonal average) in (c) summer and (d) winter.

storms, which in turn may be linked to the Southern Annular Mode (SAM), the leading mode of atmospheric variability in the Southern Hemisphere (Thompson and Wallace, 2000). The large-scale extratropical atmospheric pressure anomalies, associated with the SAM, can modulate mid-latitude pressure systems and alter wind strength and position, which could affect storm activity (Tamsitt et al., 2020; Yang et al., 2022; Campbell and Renwick, 2023). In other words, the impact of SAM on Southern Ocean Q_{net}, SST, and MLD may be manifested through low-frequency fluctuations in synoptic events. Quantifying the interaction between these disparate scales is crucial to predict future changes under anthropogenic forcing.

3.3. Eddy impacts

Eddy-driven air–sea flux anomalies are strongly regional and enhanced in areas with high climatological EKE (**Figure 8**). In energetic locations, like the Brazil–Malvinas Confluence and Agulhas Retroflection, eddies can account for up to 20% of the total turbulent heat-flux variability (Pezzi et al., 2005; Villas Bôas et al., 2015). Their contribution is largely due to the SST signature of mesoscale processes (Small et al., 2008); cyclonic eddies are associated with negative SST anomalies, while anticylonic eddies correspond to positive anomalies (Frenger et al., 2013). These SST anomalies lead to modification of the sensible heat flux via changes in the air–sea temperature gradient, and the latent heat flux, because the saturation humidity depends on temperature (Seo et al., 2023). Furthermore, these flux anomalies may contribute significantly to the upper ocean heat budget (Dong et al., 2008; Villas Bôas et al., 2015) and to variability in near-surface wind, cloud properties, and rainfall (O'Neill et al., 2003; Liu et al., 2007; Frenger et al., 2013; Rouault et al., 2016).

Here, we have assessed the impact of mesoscale eddies on air–sea heat fluxes using B-SOSE output. This model was utilized because it has finer horizontal resolution than the reanalysis data, which do not resolve the Rossby radius throughout most of the Southern Ocean. We applied an eddy tracking algorithm (Frenger et al., 2013) to B-SOSE

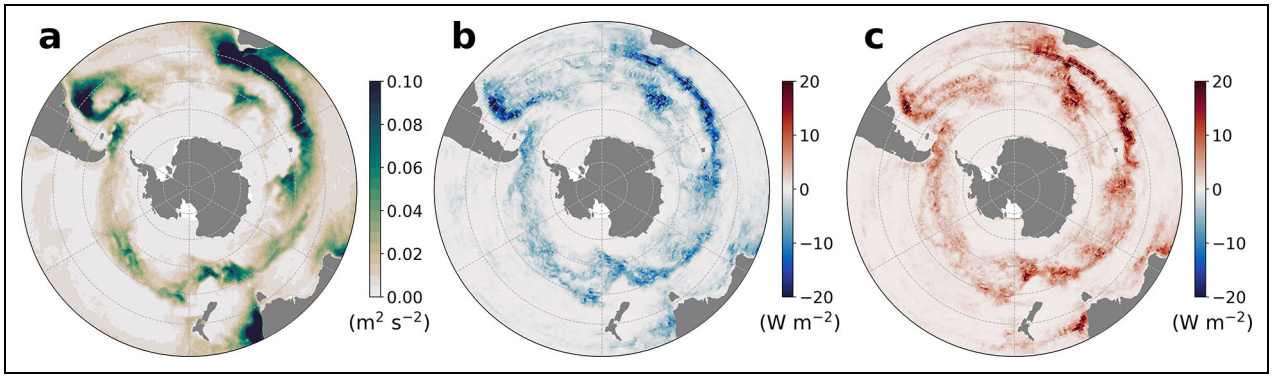

Figure 8. Eddy-driven heat-flux anomalies. Mean values, for the period 2013–2018, of (a) eddy kinetic energy derived from satellite altimetry, and high-frequency air–sea heat-flux anomalies associated with (b) cyclonic and (c) anticyclonic eddies.

sea surface height data. Unsurprisingly, coherent eddies are more prevalent in regions of high EKE (**Figure 8**). The corresponding high-frequency Q_{net} anomalies show patterns similar to those described by Villas Bôas et al. (2015). Namely, negative and positive flux anomalies are associated with cyclonic and anticyclonic eddies, respectively (**Figure 8**). The magnitude of these anomalies averaged across the whole Southern Ocean is only 2 W m^{-2}, but can be as high as 18 W m^{-2} in energetic regions. For example, in the Brazil-Malvinas Confluence, SST anomalies associated with a warm core eddy were linked to strong turbulent fluxes that influenced the stability of the marine atmospheric boundary layer (Pezzi et al., 2021). However, the extent to which opposite-signed anomalies from cyclonic and anticyclonic eddies cancel each other at annual time scales remains an open question. Future work should quantify the impact of eddies on the mean flux. For example, locations with high EKE and Q_{net} variance also closely match areas with negative mean Q_{net} values (**Figure 1**), although the mechanisms driving this pattern are not clear. Furthermore, eddy-wind feedbacks may have a differential effect on the flux anomalies associated with cyclonic and anticyclonic eddies (Rouault et al., 2016).

4. Conclusions

The Southern Ocean is vital to the total oceanic heat uptake (Frölicher et al., 2015; Huguenin et al., 2022). Thus, expanding observational coverage of air–sea fluxes in this region has global consequences (Swart et al., 2019). Long-term time series from flux moorings are critical to untangle the different scales of variability. However, Wei et al. (2020) showed that even eight hypothetical moorings in the Southern Ocean could only resolve up to 25% of the high-frequency Q_{net} variability. With new observing platforms, including uncrewed surface vehicles (USVs), a broader range of phenomena can be captured than ever before (Zhang et al., 2023). Such advances are particularly important given the growing evidence that high-frequency fluxes rectify onto longer time scales (Ogle et al., 2018; Cronin et al., 2019; Yang et al., 2022). Coordinated USV deployments could help constrain the processes operating at synoptic scales and mesoscales, as well as their larger-scale impacts. Planning these deployments, however, requires knowledge of the statistics of the air–sea flux variability. Here, we have shown, using reanalysis data and model output, that high-frequency Q_{net} fluctuations in the Southern Ocean exhibit regional and seasonal patterns, which are summarized below.

In the low-latitude Southern Ocean, high-frequency Q_{net} variability is likely driven by synoptic storms, except in boundary current regions where mesoscale eddies dominate. For example, in the Brazil–Malvinas Confluence and Agulhas Retroflection, eddies explain up to 20% of the total turbulent heat-flux variance (Villas Bôas et al., 2015). However, the extent to which opposite-signed heat-flux anomalies within cyclonic and anticyclonic eddies compensate at annual time scales remains unclear, and will depend on their relative frequency (Auger et al., 2023). Storms, by contrast, systematically cool the upper ocean at most locations. North of 45°S, storms are infrequent but cause intense cooling; the storm-driven air–sea flux anomalies at these latitudes are similar to or greater in amplitude than the seasonal cycle. Further south, in the ACC, storms are persistent (>50% of days), although the associated heat-flux anomalies are smaller, and even positive in the subpolar Atlantic and Indian sectors. This storm-induced warming is not well-understood, but seems to vary seasonally. Additionally, storm activity, in general, shows clear seasonality, peaking in winter at all latitudes.

Storm- and eddy-driven processes may also interact to control air–sea flux variability. For example, eddy-driven flux anomalies can alter cloud formation and storm development (Bharti et al., 2019; Pezzi et al., 2021). Furthermore, increased wind stress during storm events can enhance the flux anomalies associated with eddies, although the precise nature of this effect may vary between cyclonic and anticyclonic eddies (Rouault et al., 2016). At the submesoscale, storms can also modulate upper-ocean variability via wind-front interactions (du Plessis et al., 2019), which then imprints onto the air–sea fluxes (Yang et al., 2024). Numerous mechanisms operating at the submesoscale lead to high-frequency Q_{net} variability (Thomson and Girton, 2017; Swart et al., 2019; 2023; Strobach et al., 2022; Yang et al., 2024), although they have not been discussed in this study as they are not resolved in the reanalysis data or in B-SOSE.

Our results have implications for observing air–sea fluxes in the Southern Ocean. In order to obtain one measurement per decorrelation scale from an array of flux observing platforms, different sampling strategies need to be used in different regions. Throughout most of the Southern Ocean, 1–3 platforms sampling at daily intervals per $5^\circ \times 5^\circ$ box may be sufficient to resolve much of the high-frequency flux variability. However, in energetic boundary currents where decorrelation length scales are substantially shorter, multiple platforms per $1^\circ \times 1^\circ$ box might be necessary to capture the high-frequency signal. Sustaining this type of high-resolution sampling scheme poses logistical challenges, but networks of sampling in key regions are needed to further investigate the transitions and statistics on <100 km scales. Some priorities stemming from this analysis include:

- Coordinated deployment of USVs in key boundary current regions should examine the mechanisms of storm- and eddy-driven air–sea flux variability, as well as storm-eddy interactions.
- Given the meridional and seasonal variations in storm activity, targeted field observations should characterize synoptic air–sea flux variability across different latitude bands and seasons.
- Eddy-resolving multi-year model simulations should be utilized to quantify the rectification of storm- and eddy-driven air–sea flux anomalies onto the low-frequency variability.

Resolving high-frequency Q_{net} fluctuations is made difficult by the small decorrelation length and time scales, which require dense measurements to observe. Furthermore, the space and time scales of the upper-ocean response to surface forcing do not necessarily match those of the air–sea fluxes. Therefore, determining the comprehensive impact of storms and eddies necessitates sampling both the air–sea interface and the upper water column. This coordinated sampling is critical to accurately assess the impact of high-frequency air–sea fluxes on large-scale mixed-layer tracer budgets. Consistent with past work (e.g., Ogle et al., 2018; Nicholson et al., 2022; Carranza et al., 2024), our results suggest that storms contribute to the seasonal and longer-term variations in air–sea exchange. Future work should further clarify the processes that lead to spatiotemporal patterns in storm activity, which is presumably tied to the SAM (Hell et al., 2021) and basin asymmetry in the mean flux (Josey et al., 2023). Understanding these scale interactions through enhanced observations will help to improve models and reanalysis products, which are necessary to predict long-term changes in the climate system.

Data accessibility statement

All data used in this study are publicly available. Air–sea heat fluxes from the ERA5 reanalysis are available at http://cds.climate.copernicus.eu/, CCMP winds are available at http://remss.com/measurements/ccmp/, NOAA OI SST Version 2 is available at http://psl.noaa.gov/data/gridded/data.noaa.oisst.v2.highres.html, SLA from the Copernicus Marine Service altimetry product is available at http://doi.org/10.48670/moi-00148, SOFS mooring data is available at http://researchdata.edu.au/imos-deep-water-delayed-mode/959767, and B-SOSE output is available at http://sose.ucsd.edu. The eddy tracking code is available at http://github.com/jfaghm/OceanEddies.

Supplemental files

The supplemental files for this article can be found as follows:

SOFLUX_Supplementary (PDF)

Acknowledgments

Thanks to the Southern Ocean Fluxes (SOFLUX) and Observing System Design (OSD) Capability Working Groups of the Southern Ocean Observing System (SOOS) for motivating this work. We would also like to acknowledge the enormous effort it takes to deploy, recover and maintain the Southern Ocean Flux Station (SOFS) mooring. Finally, thanks to Ivy Frenger for compiling several eddy tracking algorithms and making the code publicly available (see Data Accessibility Statement).

Funding

CJP was funded by a NOAA Climate and Global Change Postdoctoral Fellowship and a Fulbright U.S. Scholar Award. SS and MDdP have received funding from the European Union's Horizon Europe ERC Synergy Grant programme under grant agreement No. 101118693 (WHIRLS), and from the Horizon 2020 Research and Innovation Program under grant agreement No. 821001 (SO-CHIC). SS is also supported by a Wallenberg Academy Fellowship (WAF 2015.0186) and the Swedish Research Council (VR 2019-04400). STG and MRM were supported by NSF award OPP-1936222 to the Southern Ocean Carbon and Climate Observations and Modeling project. STG also received support from NASA MEASURES program award 80NSSC24M0010 and from NASA's Earth System Explorers program contract 80GSFC24CA067.

Competing interests

The authors declare that they have no competing interests.

Author contributions

Contributed to conception and design: CJP, MDdP, MRM, SS, STG.

Contributed to analysis and interpretation of data: All authors.

Drafted and/or revised the article: CJP with input from all authors.

Approved the submitted version for publication: All authors.

References

Atlas, R, **Hoffman, RN**, **Ardizzone, J**, **Lediner, SM**, **Jusem, JC**, **Smith, DK**, **Gombos, D.** 2011. A cross-calibrated, multiplatform ocean surface wind velocity product for meteorological and oceanographic applications. *Bulletin of the American Meteorological Society* **92**(2): 157–174.

Auger, M, **Sallée, JB**, **Thompson, AF**, **Pauthenet, E**, **Prandi, P.** 2023. Southern Ocean ice-covered eddy properties from satellite altimetry. *Journal of Geophysical Research: Oceans* **128**(4): e2022JC019363.

Bharti, V, **Fairall, CW**, **Blomquist, BW**, **Huang, Y**, **Protat, A**, **Sullivan, PP**, **Siems, ST**, **Manton, MJ.** 2019. Air–sea heat and momentum fluxes in the Southern Ocean. *Journal of Geophysical Research: Atmospheres* **124**(23): 12426–12443.

Bourassa, MA, **Gille, ST**, **Bitz, C**, **Carlson, D**, **Cerovečki, I**, **Clayson, CA**, **Cronin, MF**, **Drennan, WM**, **Fairall, CW**, **Hoffman, RN**, **Magnusdottir, G**, **Pinker, RT**, **Renfrew, IA**, **Serreze, M**, **Speer, K**, **Talley, LD**, **Wick, GA.** 2013. High-latitude ocean and sea ice surface fluxes: Challenges for climate research. *Bulletin of the American Meteorological Society* **94**(3): 403–423.

Butterworth, B, **Miller, SD.** 2016. Air–sea exchange of carbon dioxide in the Southern Ocean and Antarctic marginal ice zone. *Geophysical Research Letters* **43**(13): 7223–7230.

Campbell, I, **Renwick, JA.** 2023. Southern Hemisphere storm tracks and large-scale variability: What do the latest reanalyses say? *Journal of Climate* **36**(16): 5549–5567.

Carranza, MM, **Gille, ST**, **Franks, PJS**, **Johnson, KS**, **Pinkel, R**, **Girton, JB.** 2018. When mixed layers are not mixed: Storm-driven mixing and bio-optical vertical gradients in mixed layers of the Southern Ocean. *Journal of Geophysical Research: Oceans* **123**(10): 7264–7289.

Carranza, MM, **Long, MC**, **Di Luca, A**, **Fassbender, AJ**, **Johnson, KS**, **Takeshita, Y**, **Mongwe, P**, **Turner, KE.** 2024. Extratropical storms induce carbon outgassing over the Southern Ocean. *NPJ Climate and Atmospheric Science* **7**(1): 106.

Cerovečki, I, **Talley, LD**, **Mazloff, MR.** 2011. A comparison of Southern Ocean air–sea buoyancy flux from an ocean state estimate with five other products. *Journal of Climate* **24**(24): 6283–6306.

Chamberlain, P, **Talley, LD**, **Cornuelle, B**, **Mazloff, MR**, **Gille, ST.** 2023. Optimizing the biogeochemical Argo float distribution. *Journal of Atmospheric and Oceanic Technology* **40**(11): 1355–1379.

Chu, WU, **Mazloff, MR**, **Verdy, A**, **Purkey, SG**, **Cornuelle, BD.** 2024. Optimizing observational arrays for biogeochemistry in the tropical Pacific by estimating correlation lengths. *Limnology and Oceanography: Methods* **22**(11): 840–852.

Cronin, MF, **Gentemann, CL**, **Edson, J**, **Ueki, I**, **Bourassa, M**, **Brown, S**, **Clayson, CA**, **Fairall, CW**, **Farrar, JT**, **Gille, ST**, **Gulev, S**, **Josey, SA**, **Kato, S**, **Katsumata, M**, **Kent, E**, **Krug, M**, **Minnett, PJ**, **Parfitt, R**, **Pinker, RT**, **Stackhouse, PW**, **Swart, S**, **Tomita, H**, **Vandemark, D**, **Weller, RA**, **Yoneyama, K**, **Yu, L**, **Zhang, D.** 2019. Air–sea fluxes with a focus on heat and momentum. *Frontiers in Marine Science* **6**: 430.

Dong, S, **Sprintall, J**, **Gille, ST**, **Talley, LD.** 2008. Southern Ocean mixed-layer depth from Argo float profiles. *Journal of Geophysical Research: Oceans* **113**(C6): C06013.

du Plessis, MD, **Swart, S**, **Ansorge, IJ**, **Mahadevan, A**, **Thompson, AF.** 2019. Southern Ocean seasonal restratification delayed by submesoscale wind-front interactions. *Journal of Physical Oceanography* **49**(4): 1035–1053.

du Plessis, MD, **Swart, S**, **Biddle, LC**, **Giddy, IS**, **Monteiro, PMS**, **Reason, CJC**, **Thompson, AF**, **Nicholson, SA.** 2023. The daily-resolved Southern Ocean mixed layer: Regional contrasts assessed using glider observations. *Journal of Geophysical Research: Oceans* **127**(4): e2021JC017760.

Frenger, I, **Gruber, N**, **Knutti, R**, **Münnich, M.** 2013. Imprint of Southern Ocean eddies on winds, clouds and rainfall. *Nature Geoscience* **6**(8): 608–612.

Frölicher, TL, **Sarmiento, JL**, **Paynter, DJ**, **Dunne, JP**, **Krasting, JP**, **Winton, M.** 2015. Dominance of Southern Ocean in anthropogenic carbon and heat uptake in CMIP5 models. *Journal of Climate* **28**(2): 862–886.

Gille, ST, **Josey, S**, **Swart, S.** 2016. New approaches for air-sea fluxes in the Southern Ocean. *Eos* **97**: 2016EO052243.

Hell, MC, **Cornuelle, BD**, **Gille, ST**, **Lutsko, NJ.** 2021. Time-varying empirical probability densities of Southern Ocean surface winds: Linking the leading mode to SAM and quantifying wind product differences. *Journal of Climate* **34**(13): 5497–5522.

Hersbach, H, **Bell, B**, **Berrisford, P**, **Hirahara, S**, **Horányi, A**, **Munoz-Sabater, J**, **Nicolas, J**, **Peubey, C**, **Radu, R**, **Schepers, D**, **Simmons, A**, **Soci, C**, **Abdalla, S**, **Abellan, X**, **Balsamo, G**, **Bechtold, P**, **Biavati, G**, **Bidlot, J**, **Bonavita, M**, **De Chiara, G**, **Dahlgren, P**, **Dee, D**, **Diamantakis, M**, **Dragani, R**, **Flemming, J**, **Forbes, R**, **Fuentes, M**, **Geer, A**, **Haimberger, L**, **Healy, S**, **Hogan, RJ**, **Hólm, E**, **Janisková, M**, **Keeley, S**, **Laloyaux, P**, **Lopez, P**, **Lupu, C**, **Radnoti, G**, **de Rosnay, P**, **Rozum, I**, **Vamborg, F**, **Villaume, S**, **Thépaut, JN.** 2020. The ERA5 global reanalysis. *Quaterly Journal of the Royal Meteorological Society* **146**(730): 1999–2049.

Hodges, KI, **Lee, RW**, **Bengtsson, L.** 2011. A comparison of extratropical cyclones in recent reanalyses ERA-Interim, NASA MERRA, NCEP CFSR, and JRA-25. *Journal of Climate* **24**(18): 4888–4906.

Huang, B, **Liu, C**, **Banzon, V**, **Freeman, E**, **Graham, G**, **Hankins, B**, **Smith, T**, **Zhang, HM.** 2021. Improvements of the Daily Optimum Interpolation Sea Surface Temperature (DOISST) version 2.1. *Journal of Climate* **34**(8): 2923–2939.

Huguenin, MF, **Holmes, RM**, **England, MH.** 2022. Drivers and distribution of global ocean heat uptake over the last half century. *Nature Communications* **13**(1): 4921.

Josey, SA, **Grist, JP**, **Mecking, JV**, **Moat, BI**, **Schulz, E.** 2023. A clearer view of Southern Ocean air-sea interaction using surface heat flux asymmetry. *Philosophical Transactions of the Royal Society A:*

Mathematical, Physical, and Engineering Sciences **381**(2246): 20220067.

Kamenkovich, I, **Haza, A**, **Gray, AR**, **Dufour, CO**, **Garraffo, Z.** 2017. Observing system simulation experiments for an array of autonomous biogeochemical profiling floats in the Southern Ocean. *Journal of Geophysical Research: Oceans* **122**(9): 7595–7611.

King, JC, **Marshall, GJ**, **Colwell, S**, **Arndt, S**, **Allen-Sader, C**, **Phillips, T.** 2022. The performance of ERA-Interim and ERA5 atmospheric reanalyses over Weddell Sea pack ice. *Journal of Geophysical Research: Oceans* **127**(9): e2022JC018805.

Liu, WT, **Xie, X**, **Niiler, PP.** 2007. Ocean–atmosphere interaction over Agulhas extension meanders. *Journal of Climate* **20**(23): 5784–5797.

Marshall, J, **Adcroft, A**, **Hill, C**, **Perelman, L**, **Heisey, C.** 1997. A finite-volume, incompressible Navier Stokes model for studies of the ocean on parallel computers. *Journal of Geophysical Research: Oceans* **102**(C3): 5753–5766.

Mazloff, MR, **Cornuelle, BD**, **Gille, ST**, **Verdy, A.** 2018. Correlation lengths for estimating the large-scale carbon and heat content of the Southern Ocean. *Journal of Geophysical Research: Oceans* **123**(2): 883–901.

Monteiro, PMS, **Gregor, L**, **Lévy, M**, **Maenner, S**, **Sabine, CL**, **Swart, S.** 2015. Intraseasonal variability linked to sampling alias in air–sea CO_2 fluxes in the Southern Ocean. *Geophysical Research Letters* **42**(20): 8507–8514.

Nakamura, H, **Shimpo, A.** 2004. Seasonal variations in the Southern Hemisphere storm tracks and jet streams as revealed in a reanalysis dataset. *Journal of Climate* **17**(9): 1828–1844.

Nicholson, SA, **Whitt, DB**, **Fer, I**, **du Plessis, M**, **Lebehot, AD**, **Swart, S**, **Sutton, AJ**, **Monteiro, PMS.** 2022. Storms drive outgassing of CO_2 in the subpolar Southern Ocean. *Nature Communications* **13**(1): 158.

Ogle, SE, **Tamsitt, V**, **Josey, SA**, **Gille, ST**, **Cerovečki, I**, **Talley, LD**, **Weller, RA.** 2018. Episodic Southern Ocean heat loss and its mixed layer impacts revealed by the farthest south multiyear surface flux mooring. *Geophysical Research Letters* **45**(10): 5002–5010.

O'Neill, LW, **Chelton, DB**, **Esbensen, SK.** 2003. Observations of SST-induced perturbations of the wind stress field over the Southern Ocean on seasonal timescales. *Journal of Climate* **16**(10): 2340–2354.

Pezzi, LP, **de Souza, RB**, **Dourado, MS**, **Garcia, CAE**, **Mata, MM**, **Silva-Dias, MAF.** 2005. Ocean–atmosphere in situ observations at the Brazil-Malvinas Confluence region. *Geophysical Research Letters* **32**(22): L22603.

Pezzi, LP, **de Souza, RB**, **Santini, MF**, **Miller, AJ**, **Carvalho, JT**, **Parise, CK**, **Quadro, MF**, **Rosa, EB**, **Justino, F**, **Sutil, UA**, **Cabrera, MJ**, **Babanin, AV**, **Voermans, J**, **Nascimento, EL**, **Alves, RCM**, **Munchow, GB**, **Rubert, J.** 2021. Oceanic eddy-induced modifications to air–sea heat and CO_2 fluxes in the Brazil-Malvinas Confluence. *Scientific Reports* **11**(1): 10648.

Potter, GL, **Carriere, L**, **Hertz, J**, **Bosilovich, M**, **Duffy, D**, **Lee, T**, **Williams, DN.** 2018. Enabling reanalysis research using the Collaborative Reanalysis Technical Environment (CREATE). *Bulletin of the American Meteorological Society* **99**(4): 677–687.

Prend, CJ, **Keerthi, MG**, **Lévy, M**, **Aumont, O**, **Gille, ST**, **Talley, LD.** 2022. Sub-seasonal forcing drives year-to-year variations of Southern Ocean primary productivity. *Global Biogeochemical Cycles* **36**(7): e2022GB007329.

Resplandy, L, **Boutin, J**, **Merlivat, L.** 2014. Observed small spatial scale and seasonal variability of the CO_2 system in the Southern Ocean. *Biogeosciences* **11**(1): 75–90.

Rodrigues, CCF, **Santini, MF**, **Lima, LS**, **Sutil, UA**, **Carvalho, JT**, **Cabrera, MJ**, **Rosa, EB**, **Burns, JW**, **Pezzi, LP.** 2023. Air–sea exchange of carbon dioxide in the Southern Ocean and Antarctic marginal ice zone. *Anais da Academia Brasileira de Ciências* **95**: e20220652.

Roemmich, D, **Church, J**, **Gilson, J**, **Monselesan, D**, **Sutton, P**, **Wijffels, S.** 2015. Unabated planetary warming and its ocean structure since 2006. *Nature Climate Change* **5**: 240–245.

Rouault, M, **Verley, P**, **Backeberg, B.** 2016. Wind changes above warm Agulhas Current eddies. *Ocean Science* **12**(2): 495–506.

Schulz, EW, **Josey, SC**, **Verein, R.** 2012. First air–sea flux mooring measurements in the Southern Ocean. *Geophysical Research Letters* **39**(16): L16606.

Seo, H, **O'Neill, LW**, **Bourassa, MA**, **Czaja, A**, **Drushka, K**, **Edson, JB**, **Fox-Kemper, B**, **Frenger, I**, **Gille, ST**, **Kirtman, BP**, **Minobe, S**, **Pendergrass, AG**, **Renault, L**, **Roberts, MJ**, **Schneider, N**, **Small, RJ**, **Stoffelen, A**, **Wang, Q.** 2023. Ocean mesoscale and frontal-scale ocean–atmosphere interactions and influence on large-scale climate: A review. *Journal of Climate* **36**(7): 1981–2013.

Small, RJ, **de Szoeke, SP**, **Xie, SP**, **O'Neill, L**, **Seo, H**, **Song, Q**, **Cornillon, P**, **Spall, M**, **Minobe, S.** 2008. Air–sea interaction over ocean fronts and eddies. *Dynamics of Atmospheres and Oceans* **45**(3–4): 274–319.

Strobach, E, **Klein, P**, **Molod, A**, **Fahad, AA**, **Trayanov, A**, **Menemenlis, D**, **Torres, H.** 2022. Local air–sea interactions at ocean mesoscale and submesoscale in a Western boundary current. *Geophysical Research Letters* **49**(7): e2021GL097003.

Swart, S, **du Plessis, M**, **Nicholson, SA**, **Monteiro, PMS**, **Dove, LA**, **Thomalla, S**, **Thompson, AF**, **Biddle, LC**, **Edholm, JM**, **Giddy, I**, **Heywood, KJ**, **Lee, C**, **Mahadevan, A**, **Shilling, G**, **de Souza, RB.** 2023. The Southern Ocean mixed layer and its boundary fluxes: Fine-scale observational progress and future research priorities. *Philosophical Transactions of the Royal Society A: Mathematical, Physical, and Engineering Sciences* **381**(2249): 20220058.

Swart, S, **Gille, ST**, **Delille, B**, **Josey, S**, **Mazloff, M**, **Newman, L**, **Thompson, AF**, **Thomson, J**, **Ward, B**, **du Plessis, M**, **Kent, EC**, **Girton, J**, **Gregor, L**, **Heil, P**, **Hyder, P**, **Pezzi, LP**, **de Souza, RB**, **Tamsitt, V**, **Weller, RA**, **Zappa, CJ.** 2019. Constraining Southern Ocean air-sea-ice fluxes through enhanced observations. *Frontiers in Marine Science* **6**: 421.

Tamsitt, V, **Cerovečki, I**, **Josey, SA**, **Gille, ST**, **Schulz, E.** 2020. Mooring observations of air-sea heat fluxes in two Subantarctic Mode Water formation regions. *Journal of Climate* **33**(7): 2757–2777.

Thompson, DWJ, **Wallace, JM.** 2000. Annular modes in the extratropical circulation. Part I: Month-to-month variability. *Journal of Climate* **13**(5): 1000–1016.

Thomson, J, **Girton, J.** 2017. Sustained measurements of Southern Ocean air–sea coupling from a Wave Glider autonomous surface vehicle. *Oceanography* **30**(2): 104–109.

Verdy, A, **Mazloff, MR.** 2017. A data assimilating model for estimating Southern Ocean biogeochemistry. *Journal of Geophysical Research: Oceans* **122**(9): 6968–6988.

Villas Bôas, AB, **Sato, OT**, **Chaigneau, A**, **Castelão, GP.** 2015. The signature of mesoscale eddies on the air–sea turbulent heat fluxes in the South Atlantic Ocean. *Geophysical Research Letters* **42**(6): 1856–1862.

Wei, Y, **Gille, ST**, **Mazloff, MR**, **Tamsitt, V**, **Swart, S**, **Chen, D**, **Newman, L.** 2020. Optimizing mooring placement to constrain Southern Ocean air–sea fluxes. *Journal of Atmospheric and Oceanic Technology* **37**(8): 1365–1385.

Whitt, DB, **Nicholson, SA**, **Carranza, MM.** 2019. Global impacts of subseasonal (<60 day) wind variability on ocean surface stress, buoyancy flux, and mixed layer depth. *Journal of Geophysical Research: Oceans* **124**(12): 8798–8831.

Williams, RG, **Ceppi, P**, **Roussenov, V**, **Katavouta, A**, **Meijers, AJS.** 2023. The role of the Southern Ocean in the global climate response to carbon emissions. *Philosophical Transactions of the Royal Society A: Mathematical, Physical, and Engineering Sciences* **381**(2249): 20220062.

Yang, H, **Chen, Z**, **Sun, S**, **Li, M**, **Cai, W**, **Wu, L**, **Cai, J**, **Sun, B**, **Ma, K**, **Ma, X**, **Jing, Z**, **Gan, B.** 2024. Observations reveal intense air–sea exchanges over submesoscale ocean front. *Geophysical Research Letters* **51**(2): e2023GL106840.

Yang, J, **Cheng, X**, **Qin, J**, **Zhou, G**, **Li, L**. 2022. The synoptic and interannual variability of extreme turbulent heat flux events during austral winter in the southern Indian Ocean. *Journal of Geophysical Research: Atmospheres* **127**: e2021JD035792. DOI: https://doi.org/10.1029/2021JD035792.

Zhang, D, **Chiodi, AM**, **Zhang, C**, **Foltz, GR**, **Cronin, MF**, **Mordy, CW**, **Cross, J**, **Cokelet, ED**, **Zhang, JA**, **Meinig, C**, **Lawrence-Slavas, N**, **Stabeno, PJ**, **Jenkins, R.** 2023. Observing extreme ocean and weather events using innovative saildrone uncrewed surface vehicles. *Oceanography* **36**(2–3): 70–77.

How to cite this article: Prend, CJ, du Plessis, MD, Mazloff, MR, Sunnercrantz, L, Swart, S, Gille, ST. 2025. Observing system requirements for measuring high-frequency air–sea fluxes in the Southern Ocean. *Elementa: Science of the Anthropocene* 13(1). DOI: https://doi.org/10.1525/elementa.2024.00061

Domain Editor-in-Chief: Jody W. Deming, University of Washington, Seattle, WA, USA

Guest Editor: Luciano Ponzi Pezzi, Instituto Nacional de Pesquisas Espaciais, Sao Jose dos Campos, São Paulo, Brazil

Knowledge Domain: Ocean Science

Part of an Elementa Special Feature: Understanding the Trajectory and Implication of a Changing Southern Ocean: The Need for an Integrated Observing System

Published: March 19, 2025 **Accepted:** January 31, 2025 **Submitted:** September 27, 2024